An Electro-Optical Imaging Approach to the Prompt Signal Processing Problem of Mega-Channel SSC Detector Arrays

Mark Lowry, Eldon Ables, Richard Bionta, Ron Haigh,
Keith Hugenberg, Ralph Kalibjian, Charles McConaghy,
Darin Milton, Mark Rotter, and Hal Schulte

This paper was prepared for submittal to the
Symposium on Detector Research and Development for the
Superconducting Super Collider
Fort Worth, TX
October 15-18, 1990

December 1990

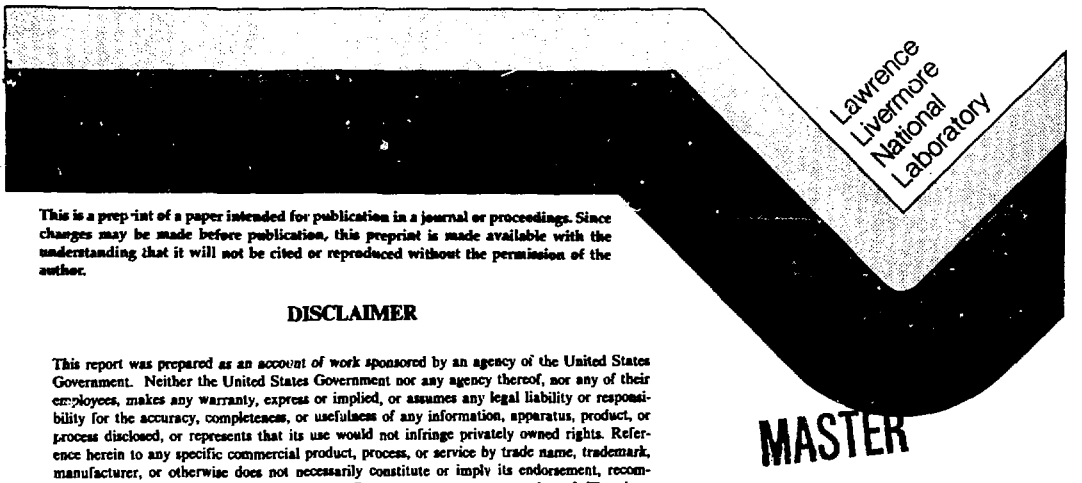

UCRL-JC--105645

DE91 008739

An Electro-Optical Imaging Approach to the Prompt Signal Processing Problem of Mega-Channel SSC Detector Arrays

Mark Lowry, Eldon Ables, Richard Bionta, Ron Haigh, Keith Hugenberg,
Ralph Kalibjian, Charles McConaghy, Darin Milton, Mark Rotter, and Hal Schulte
Lawrence Livermore National Laboratory
Livermore, California 94550

Introduction

The physics demands of high luminosity at the SSC and the sometimes subtle measurements required to elucidate new physics will undoubtedly tax existing instrumentation. As is the case with most experimental fields, new physics follows from better measurement concepts and technologies. We expect this to be the case with the SSC as well. In what follows, we offer a glimpse of what may be possible using some of the recent results from the emerging technologies in the field of electro-optics.

A Proposed Electro-Optic System Architecture

The large number of channels required for SSC instrumentation and the temporal resolution required lead quite naturally to the consideration of electro-optical imaging techniques.[1] This is particularly true with the need to establish reliable and prompt event triggers that are based upon total energy and event topology, as we shall see with the system outlined in Figure 1.

Here we start with more-or-less conventional HEP detectors that yield charge as the measurement output. This charge is then used to modulate an externally provided optical carrier signal (amplifiers and pulse shaping may not even be required, as will be seen in what follows). The basic ideas regarding the optical modulator are discussed in ref. 1. The optical carrier may be supplied by some, hopefully small, number of fibers that provide optical power to a chip containing many of the modulators discussed in ref. 1. The optical power division is accomplished on a chip as well (perhaps monolithically integrated with the modulator chip). This large

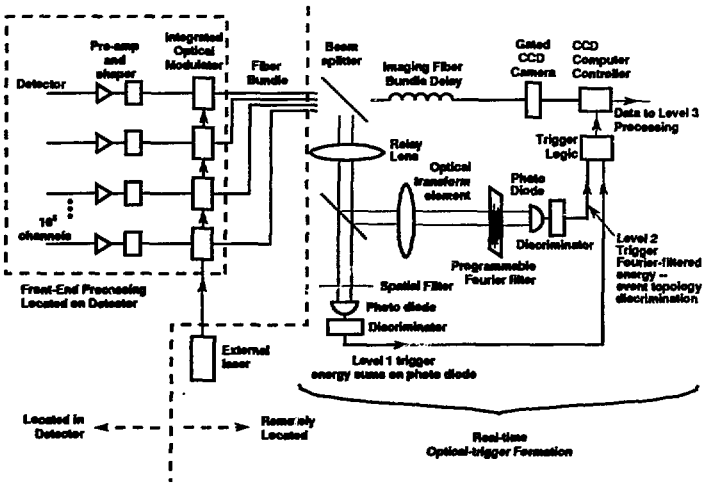

Figure 1. Proposed electro-optic system architecture for high luminosity data acquisition at the SSC. Some key features are the use of ultra-sensitive integrated-optical modulators and the use of optical pattern recognition for trigger formation.

* This work was performed under the auspices of the U.S. Department of Energy by the Lawrence Livermore National Laboratory under contract number W-7405-ENG-48.

number of independent optical channels (perhaps as many as 100 are possible per chip) are brought off chip in individual optical fibers. These optical fibers are arranged in an imaging bundle—such that image information is preserved. In the event of a hit, this bundle is then the conduit of a transient image that propagates to the level-one trigger.

The first step in the trigger generation process is to pick-off a portion of the image power through use of a conventional optical beam splitter. Let us call these beams, after the splitter, the trigger image and the major portion the record image. The trigger image can be split into two beams. In the case of data from a calorimeter, one leg of the trigger beam can be spatially filtered with a filter whose optical density is graded as, $\sin(\theta)$, where θ is the angle with respect to the beam direction for that pixel element. As this filtered image is relayed optically to a large area photodetector, the output charge from the photodiode is then a prompt measure of the total transverse energy—the delay for this part of the trigger formation is just the response time of the photodetector; a few nanoseconds is easy.

The second portion of the trigger image can be used to perform relatively complex event topology discrimination through the use of well-established optical pattern recognition techniques. The most straight-forward technique applies again to the case of calorimetry. By applying the optical Fourier transform to the second trigger image—realized conveniently with the use of simple optical lenses[2]—one can perform spatial frequency filtering operations by simply placing the appropriately patterned spatial transmission filter in the Fourier plane (by using the new technologies of spatial light modulation,[3] the characteristics of this frequency filter could be conveniently controlled electronically). The output of the spatial filter is then relayed to another large area photodetector. The prompt optical sum performed by this photodetector is a measure of the energy content only of features of the event that have a frequency content that is matched to the spatial filter in the Fourier plane. This then allows us to discriminate promptly (a few nanoseconds) on the basis of event topology, as well as total event energy. It should be noted that optical processing has at least one precedent[4] in HEP instrumentation.

Perhaps this optical pattern recognition may be extended to the case of tracking detectors. It may be possible to use the optical Hough transformation to detect the existence of stiff tracks. The Hough transformation maps straight lines into points—one coordinate of the point being the line's angle with respect to the abscissa, and the other is its distance from the origin. Using techniques similar to the optical Fourier transformation, the Hough transformation may be accomplished optically.[5,6] It may prove possible to optically correlate this trigger with the calorimeter information to provide an elegant and comprehensive trigger, promptly, and with little or no electronics in difficult environs. It must be pointed out that all the optical Hough transformation work that we have seen to date is accomplished with a mechanically rotating optical element, and thus would be far too slow for HEP instrumentation. However, there may be a way to realize the transform in optical fashion instantly, and we are currently exploring that possibility.

We have thus far painted a simple picture of Fourier optics techniques. Our laboratory measurements to date—and some reflection on the Fourier optics theory—would suggest that performing the Fourier transform of the image from an optical fiber bundle may be very difficult. Basic Fourier optics work is done with the use of simple apertures, and the optical wavefronts employed are coherent. In our case, the individual image pixels have probably suffered large relative optical phase shifts. These phase shifts lead to severe interference noise in the Fourier plane. We can suggest three possible ways around this relative phase shift problem.

First, the fact that our optical carrier was derived from a single laser (or perhaps a phase locked set of lasers) may allow us to adjust these relative phases such that when we arrive at the Fourier plane the relative phase shifts have been compensated. Further, the use of integrated optical devices as our signal encoding mechanism may provide a convenient solution. The most fundamental form of optical modulation is the phase shifter. In fact, the Mach-Zehnder modulator discussed in ref. 1 is composed of two such devices. A phase shifter could be employed in each channel to compensate these phase shifts in response to the input from a feedback mechanism. Another phase compensation technique would be the use of a holographic element in the image plane after the bundle, this element could be used to compensate the optical phases of the individual image pixels by focusing the image onto this holographic phase plate.[7] We are exploring both of these phase compensation techniques, and hope to carry-out experiments soon. Finally, the partially coherent image from the fiber bundle could be transformed into an incoherent image. This may be achieved by imaging the fiber output unto an image intensifier. The image intensifier output is then incoherent light from the phosphor screen. Then the incoherent image could be processed using incoherent processing techniques. This offers the added advantage of allowing the image information to be gated; however, to retain the speed of the optical processing fast phosphors must be used—so, the gain of the intensifier may then become an issue.

The remaining beam, the record image, can be refocused onto another imaging optical fiber bundle, and be allowed to propagate for however long is required for complete trigger formation. After trigger formation, the image is captured by a gated ultra-fast readout CCD imager. Image readout times of 10 μs for 10,000 pixels with a dynamic ranges of 1,000 are attainable with today's technology. Extended dynamic ranges could be attained by using a slightly higher power optical carrier and splitting the record image with a 10:90 beam splitter and recording both images.

The advantages of using this electro-optical imaging approach are several:

- The transmission media (small diameter optical fibers with approximately $1cm^2$ cross-sectional area per 10,000 fibers) offers low radiation scattering, and a mechanically manageable cable plan.

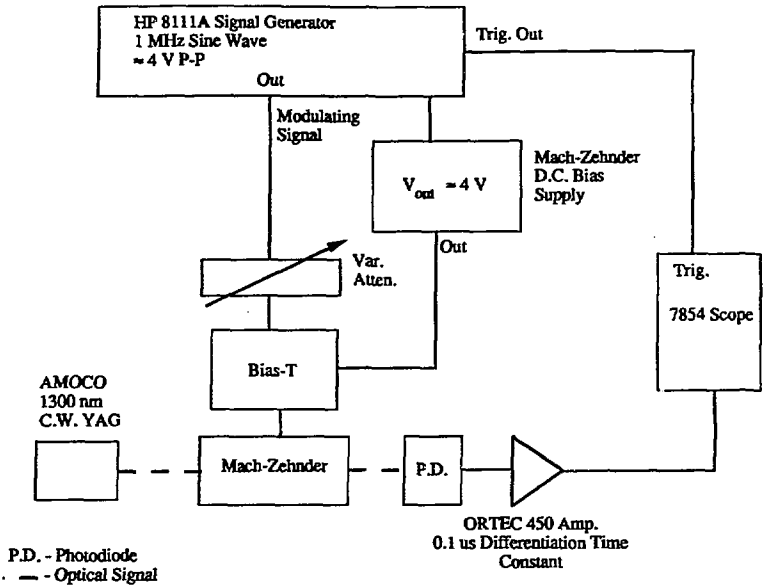

Figure 2. Experimental layout for Mach-Zehnder dynamic range measurements.

- Since all channels are brought outside in parallel, triggering architectures become very flexible and amenable to modification in the future.
- Ground-loops and other forms of EMI become less of a problem.
- The modulators and fiber medium easily support the required temporal response.
- The power consumption can be much less than 1 mW per channel for the power-dissipation critical inner-tracker applications.
- The fiber medium conveniently provides signal delay to accommodate the trigger formation time.
- The potential for operation without amplifiers (discussed in detail below) adds greatly to system reliability—particularly for the high radiation environments.
- Optical pattern recognition and optical summing techniques can be applied for prompt trigger formation.

While this total system architecture is quite attractive in many respects, we should not overlook the value of any one of the roughly three major subsystems: the optical modulators, the image processing techniques, and the fast CCD data capture. We will spend the rest of the paper addressing the optical modulators.

Integrated Optical Modulator Results

While we have been pursuing instrumentation development with modulators for several years, we have only recently considered them in the context of HEP experiments. To that end, we set out to understand how they might best be used in HEP experiments. A potential application of the technology is in calorimetry experiments, where exceptional dynamic range is required. We have made measurements of dynamic range at 800 nm, using 2x2 modulators, and measurements at 1300 nm using Mach-Zehnder modulators. Due to the limited space, we will only discuss the Mach-Zehnder measurements here.

The experimental setup is outlined in Figure 2. We used a sine-wave electrical input for convenience, but the conclusions should apply to pulse operation as well. The bandwidth of the system was limited by the amplifier at 1.5 MHz. The bias applied to the modulator was adjusted by observing the signal-to-noise of a very weak signal; at the point of maximum signal-to-noise, the bias voltage level was fixed. Figure 3 shows the result of three different levels of electrical attenuation (on the sinusoidal input signal) ranging from 0 dB to 80 dB (voltage). Even with 80 dB attenuation (x10,000), the output signal from the modulator is easily seen on the scope trace. For the 0 dB trace, the negative going portion of the sinusoidal input is distorted as it passes through the minimum

in the sinusoidal response function (see ref. 1), however the positive going portion does not go through the response peak (indicating that the modulator was not biased precisely at the half-power point). Concentrating on the positive going portion of the sinusoid, we see that the input signal goes through a dynamic range of at least 10,000. At the lowest input signal level (80 dB attenuation), the signal is still much above the noise. By analyzing the rms noise of our system with the light beam blocked, and with the beam unblocked but no modulation signal, we find that at the attenuation value of 10,000 the ratio of the peak signal to the noise due to just the laser/modulator combination is ~ 4. However, these noise measurements were made from scope traces of the same time scale as Figure 3; here the noise bandwidth is determined by the amplifier roll-off at 1.5 MHz, and the record length at the low end; we find this to be 1.3 MHz. Extrapolating to the case of a 10 MHz bandwidth (more suitable for most SSC applications), we find that this increase in bandwidth should lead to a noise increase of a factor of ≈ 2.77. Thus operating with a bandwidth of 10 MHz, we would expect to find a dynamic range of ≈ (4/2.77)(10,000) or slightly more than 14,000. Further, since we know that this signal can be linearized, we can establish a linear relationship between the optical power from the modulator and the input voltage to the modulator.

At this point, it is convenient to discuss the relationship of the charge (or voltage sensitivity) to the parameters of the carrier modulator system. The optical power output of most modulators can be conveniently described by

$$P=P_0F(V) \qquad \text{eq. 1}$$

where $P_0 = \eta P_{in}$ is the maximum carrier power out of the modulator—when F(V)=1, η is the insertion loss, P_{in} is the input optical power, and F(V) is some modulation function of charge or voltage. The uncertainty of the measured optical throughput, ∂P, is made up of three contributions: carrier power instabilities, detector noise, and amplifier noise. We may lump these uncertainties together into the total uncertainty in the measured power, ∂P. The voltage uncertainty due to fluctuations in the measured optical power is given by

$$\delta V=(\delta P/P_0)/(dF/dV) \qquad \text{eq. 2}$$

assuming that ∂P is small compared to P_0, and dF/dV is not close to zero. Any fluctuations from the modulator itself[8] are then added in quadrature with this uncertainty to arrive at the total uncertainty in the measured voltage.

For the case of the Mach-Zehnder, reproducing eq. 1 from ref. 1 we note that

$$P=\eta(1-\varepsilon f(V_s))P_{in}\sin^2\left(\frac{\pi V_s}{2V_\pi}+\phi\right)+\eta\varepsilon f(V_s)P_{in} \qquad \text{eq. 3}$$

where P is the modulated optical power output, P_{in} is the input optical power, V_S is the applied signal voltage, V_π is the voltage required to modulate from a minimum to maximum (1/2 of an interference fringe), η is the device insertion loss, ε is the low voltage modulator extinction and usually $\varepsilon < 0.01$, ϕ is

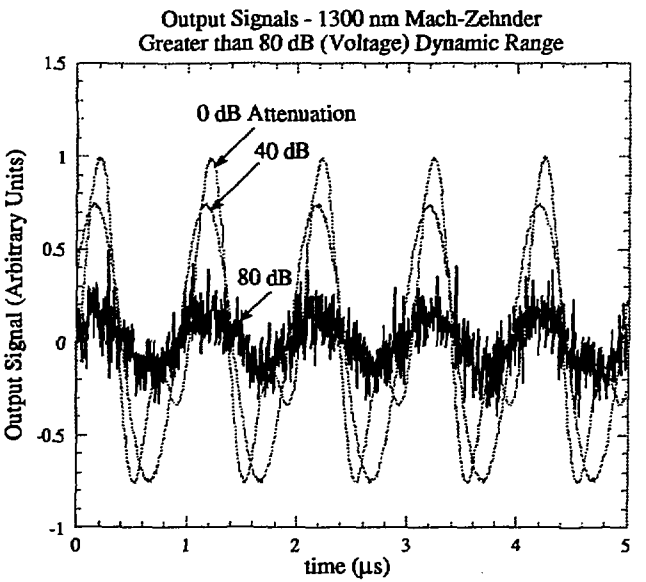

Figure 3. Results of Mach-Zehnder dynamic range measurements. A dynamic range well in excess of 10,000 is demonstrated.

the quiescent phase shift of the device, and f is a phenomenological function that describes the behavior of the modulator extinction at high modulation voltages "f" is very nearly 1 except at voltages much larger than V_π[9]. With dF/dV at its maximum (i.e., at the half-power point, in the Mach-Zehnder case), we find,

$$\frac{\delta Q}{Q_\pi} = \frac{\delta V}{V_\pi} = (\delta P/P_0)\frac{2}{\pi(1-\varepsilon)} \qquad \text{eq. 4}$$

so the voltage (charge) uncertainty is proportional to the relative optical power uncertainty, scaled by $V_\pi(Q_\pi)$.

For the measurements shown in Figure 3 extrapolated to 10 MHz, $\delta v/v_\pi$= 1/(dynamic range) = 1/14,000 = 7.1×10^{-5} Equivalently, $\delta Q/Q_\pi = 7.1\times10^{-5}$ Alternatively one may extract the relative optical power uncertainty using eq. 4, $\partial P/P_0$=1.1=10^{-4}. The modulator used for the measurements in Figure 3 was an in-house designed and fabricated high-bandwidth traveling wave Mach-Zehnder. In general, for SSC applications it appears that lumped element electrode structures may be preferred; to understand the charge sensitivity possible for SSC applications let's consider the lumped element case. Becker[10] discusses a figure-of-merit for lumped-element modulators: $M=V_\pi L$, where L is the length of the electrode structure. Becker finds that M= 14 V-mm and that the capacitance/electrode length ρ =0.85 pF/mm . Thus, one can easily calculate the amount of charge deposited on the electrode structure to yield a voltage of V_π; $Q_\pi=M\rho$=12 pC. Applying this to our dynamic range measurements above yields the result that the minimum charge that we are capable of detecting would be 12 pC/14,000 = 0.86 femtocoulombs. This assumes our value of the relative optical power uncertainty extrapolated to 10 MHz bandwidth, and the Q_π of a lumped element modulator structure. We are further making the tacit assumption that the electrode termination resistance is large enough (or actively gated) so that the charge will not dissipate on time scales consistent with the desired bandwidth.

It is useful to consider the shot noise (counting statistics) limitations on the dynamic range. For our optical power level of ~ 5 mW—at the Mach-Zehnder bias point, a projected bandwidth of 10 MHz, at a wavelength of 1300 nm, and a detector quantum efficiency of 90%, the shot noise is easily calculated using the usual Poisson distribution assumption. Given these circumstances we find that the shot noise fluctuations in the measured optical power would be 1.8×10^{-5} of the average power, i.e. $\partial P/P=1.8\times10^{-5}$, where ∂P is the fluctuations in the measured power (assuming only shot noise) and P is the average measured power. So we are a factor of 6.1 away from realizing a shot noise limited system. For the ideal optical shot-noise limited system, operating, with an optical power of 5 mW at the receiver, the charge sensitivity could be as good as 0.14 femtocoulombs. However, at these low charge levels, we are probably approaching the level of the thermal charge fluctuations in the modulator capacitance: at room temperature with a capacitance of 5 pF the thermal noise would be of order 1000 electrons or 0.16 fC (see ref. 8).

The dependence of the sensitivity on the slope of the modulation function , eq. 2, has led us to consider resonant modulator structures. These structures exhibit a modulation function that consists of resonances, i.e. the device is characterized by a "Q"—or finesse in the optical vernacular. These kinds of devices may be of interest where extremely high charge sensitivity is required but dynamic range is not. Most tracking detectors, by virtue of their necessarily small volumes, would seem to fall into this category.

This kind of modulator is very simple in design. It consists of a single waveguide with dielectric mirrors deposited on the input and output facets of the chip to form an optical cavity. The resonances in transmission are a function of the ratio of the optical length of the cavity and the optical free-space wavelength. For a Fabry-Perot modulator, the modulation function, in analogy with eq. 2 can be derived by following Born and Wolf[11] but including a loss factor,

$$G(\delta)=\frac{(1-R)^2e^{-\alpha L}}{(1-Re^{-\alpha L})^2+4Re^{-\alpha L}\sin^2(\delta/2)} \qquad \text{eq. 5}$$

where α is the optical loss coefficient, R is the reflectivity of the cavity ends, δ is the optical phase difference; $\delta=4\pi nL/\lambda$, where n is the refractive index. Electrodes are then deposited on either side of the single waveguide. The electrodes are used to modulate the index of refraction and hence the optical length of the cavity. Thus, this structure can be used as a tuneable monochromater or a very sensitive modulator that responds to applied voltage or charge.

Figure 4 shows data taken at LLNL from an integrated optical Fabry-Perot modulator of LLNL design and fabrication. Here the resonance is clearly seen. In this figure, the finesse, *F*—the ratio of the free spectral range (distance between peaks) to the FWHM of the resonance—is approximately 12. This data was acquired by scanning the optical spectrum; which is equivalent to applying a voltage or charge. One can easily relate the finesse of this device to the maximum slope of the modulation function. An analytic expression is possible from eq. 5, however, the essential point can be made with far less algebra, by approximating the resonant peaks with triangular spikes. If we constrain the peak of the spike to correspond to the peak of the resonance and also force it to pass through the FWHM of the resonance, we arrive at a very simple approximation for the slope of the resonant peak, especially for a finesse that is large,

$$\frac{dG}{dV} \approx F/(2V_\pi) \qquad \text{eq. 6}$$

where *F*- is the finesse. Applying eq. 2, we may calculate the voltage and charge uncertainties (hence, theoretical sensitivities) for the Fabry-Perot modulator as,

$$\frac{\delta Q}{Q_\pi} = \frac{\delta V}{V_\pi} = (\delta P/P_0)\frac{2}{F} \qquad \text{eq. 7}$$

Naturally, this sensitivity scales with the inverse of the finesse which can in principal be made quite high. Given the same optical noise parameters of our MZ measurements and using the finesse value from Figure 4, we would estimate under these conditions that the charge sensitivity of the FP modulator would be 0.3 femtocoulombs or ~ 2000 electrons.

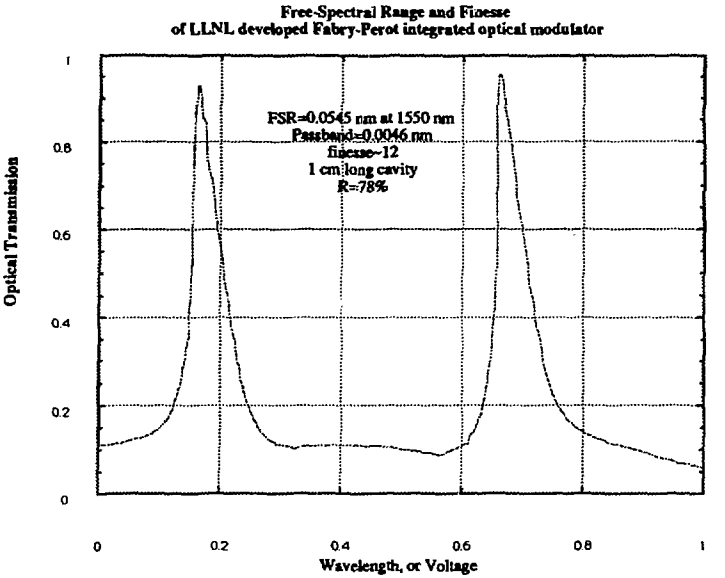

Figure 4. The modulation shape function for a Fabry-Perot structure. Note the resonant peaks in the response.

The sensitivity leverage of the resonant Fabry-Perot modulator is clear. We could presumably extract even better performance from a FP with a higher finesse and/or shot-noise limited optical detection, however we are again approaching the level of the thermal noise in the electrode structure itself (ref. 8).

A word of caution about such resonant structures is in order: Their excellent sensitivity may come at the price of significant instability, with respect to temperature in particular. However, it may be possible to compensate these instabilities with a feedback mechanism or conceive device designs that are self compensating, yet resonant—the Mach-Zehnder is an example of a self-compensating structure, unfortunately it is not resonant. The Mach-Zehnder's two parallel paths pass through the crystal so closely that any temperature-induced optical path change is experienced identically by both. Perhaps it is possible to design a resonant structure that also has this feature.

Modulator Power Dissipation

For many SSC applications, the power dissipated by subsystem elements is critical. For the case of the modulators, the dissipated power is from two sources the optical carrier and the charge driving the modulator. As we shall see, the most significant component is the optical power.

The optical power dissipation will be approximately equal to (3/2)P_0—on the order of 1/2 of the input optical power will probably be lost due to inefficiencies in optical coupling, and operation at the half power point will then account for an additional 1/2P_0.

The energy dissipated due to the modulating charge is calculated as $q^2/2C$. Since the MZ will be the least sensitive of the two devices discussed here, we will consider it as the worst case. Taking C=2.55 pF and assuming $q=Q_\pi$=12 pC, we find that there will be 28 pJ of energy dissipated per "hit," maximum. Then, if every pixel registered a hit every beam crossing, the dissipated power from the charge would be 28pJ/1.6 nS = 1.8 mW. However, since the detector elements that are not hit far outnumber those that are, on average, this power dissipation term will be reduced by a couple orders of magnitude. So we would expect the charge dissipation power to be of order 10 microWatts, or less, on average. It should be pointed out that no matter how the charge is readout the energy must be dissipated.

While on the subject of power dissipation it should be noted that given the ultimate shot-noise limited system, where the optical noise goes as the $P_0^{1/2}$, there will be a trade-off between noise--hence, sensitivity—and optical power dissipation. This tradeoff should be considered when determining the optimum modulator design for a particular SSC application.

System Costs

There is not space here for a comprehensive discussion of projected costs. However, it is clear that without significant advances in integration density (number of modu-

lators per chip) and automated packaging techniques the per channel costs will be prohibitive. We hope to pursue, with industrial partners, both of these critical areas.

Radiation Sensitivity

While some encouraging data on the radiation sensitivity of these integrated optical modulators does exist,[12] there is much that remains to be done at SSC dose-rate levels. And we have begun a program of investigation for this important issue for modulators at the SSC.

Conclusions

We have presented dynamic range, and sensitivity data for two distinct classes of integrated optical modulator. These measurements demonstrate that these devices may prove very useful for both calorimetry and tracking. Further, we have outlined a comprehensive electro-optical imaging system architecture that includes a novel and elegant optical approach to trigger formation and the means of capturing the triggered event data.

As high energy physics moves into the twenty first century with the completion of the Superconducting Super-Collider, we believe that only by incorporating the best and most sophisticated technology available will the physics move forward as efficiently as possible. We hope that we have demonstrated, in a substantive fashion, that electro-optics has a very large role to play.

Acknowledgements

We would like to thank Dan Marlow of Princeton University for many helpful discussions and much encouragement. Thanks are also due to Maged Atiya of Brookhaven for his encouragement and critical evaluation of some of these ideas. We also appreciate the time and consideration given by several researchers to some aspects of this work during a recent visit to Brookhaven: Veljko Radeka, Paul O'Connor, Venetios Polychronakos, Howard Gordon, William Willis, and Wilfred Cleland. David Nygren from Lawrence Berkeley Laboratory has also provided useful discussion and encouragement. As relative newcomers to the field, we gratefully acknowledge the help of many HEP researchers, too numerous to list, who attended the '90 Snowmass meeting and played an important role in shaping some of these ideas through their interest and constructive criticism.

We thank Richard Becker of Integrated Optics Circuit Consultants for useful discussions on modulator sensitivity.

At LLNL, we would like to thank Hye-Sook Park for her suggestion of the optical Hough transformation, Stan Thomas for useful discussions about current image intensifier technology, Wolfgang Stoeffl and Craig Wuest for their interest, and Orrin Fackler, Chip Britt, and Tony Chargin for their interest and encouragement.

References

1 M.E.Lowry, B.A.Jacoby, and H.F.Schulte, *Electro-Optic Transient Imaging Instrumentation Development at Lawrence Livermore National Laboratory: Implications for SSC Instrumentation Development*, in these proceedings (previous paper).

2 J.W.Goodman, *Introduction to Fourier Optics*, McGraw-Hill, San Francisco (1968)

3 W. P. Bleha, L. T. Lipton, E. Wiener-Auner, J. Grinberg, P. G. Reif, D. Casasent, H. B. Brown, and B. V. Markevitah, *Application of the Liquid Crystal Light Value to Real-Time Optical Data Processing*, Optical Engineering, Vol. 17, #4, pp. 371-384 (1978); note: Commercial products are now available from Hughes.

4 W. E. Cleland, D. E. Kraus, and J. A. Thompson, *Optical Trigger Processor for High Energy Physics*, Nuclear Instruments and Methods, Vol 216, #3, pp. 405-414, New-Holland, Amsterdam (1983).

5 W.H.Steier and R.K.Shori, *Optical Hough Transformation*, Applied Optics, vol. 25, # 16, pp. 2734-38, 1986

6 G.Eichmann and B.Z.Dong, *Coherent Optical Production of the Hough Transformation*, Applied Optics, vol. 22, #6, pp 830-34, 1983

7 Reynolds, Devetis, Pamert, and Thompson, *The New Physical Optics Notebook: Tutorials in Fourier Optics*, pp. 323-325, SPIE Optical Engineering Press, Bellingham, Washington (1989).

8 At least two potential sources of noise from within the modulator must be considered: The thermal noise of the electrode capacitance $\partial Q=(CkT)^{1/2}$ (integrated over all frequencies) and the ferro-electric noise from within the crystal itself. For a discussion of these two sources see D.A. Bell, *Noise and the Solid State*, Wiley (1985) At room temperature the thermal noise appears to dominate.

9 As V_S grows large, the guiding characteristics of the waveguides are altered such that one will become more lossy than the other—this leads to incomplete interference and reduced extinction at large values of V_S.

10 R. A. Becker, *Multigigahertz Lumped-Element Electro-optic Modulators*, IEEE J. Quant. El., QE-21, 8, pp 1144-1146 (1985).

11 See for instance p. 327 Born and Wolf, *Principles of Optics*, Pergamon Press, Oxford (1986) for a discussion of Fabry-Perot interferometers.

12 F. Roeske, Jr., D. R. Jander, G. D. Lancaster, M. E. Lowry, G. McWright, R. T. Peterson, and W. E. Tindall, *Preliminary Radiation Hardness Testing of Lithium Niobate Optical Directional Coupler Modulators Operating at 810 nm*, Proc. SPIE Technical Symposium Southeast on Optics, Electrooptics, and Sensors, Orlando, FL (May 1987).